Local Strain Accommodation in Polycrystalline Ni-Base Superalloys

Jennifer Walley, The Ohio State University, 477 Watts Hall, 2041 College Rd. Columbus, OH 43210, walley.7@osu.edu

Robert Wheeler, UES, Inc. 4401 North Dayton-Xenia Rd, Dayton, OH 45432

Michael D. Uchic, Air Force Research Laboratory, Materials & Manufacturing Directorate, AFRL/RXLM, Wright Patterson AFB, OH 45433

Michael J. Mills, The Ohio State University

ABSTRACT

To exploit new hybrid nickel-based superalloys, physics-based computational models are needed to predict material properties and describe material behavior during exposure to complex life cycles. Such models will allow an iterative assessment of microstructural morphology as related to mechanical properties prior to production of large-scale test specimens or components, thereby reducing development time and cost. Development of these models is currently hindered by a gap in the understanding of local deformation behavior at the intra- and intergranular level. A new in-situ experimental methodology is being developed to characterize local strain heterogeneities in nickel-based superalloys that have a relatively fine grain size (d_{ave}<50μm). Initial work has been performed on Rene 104 that was heat treated to produce two sets of samples with a similar grain size but different γ' distributions and grain boundary morphologies. One sample set had planar boundaries and a bimodal γ' distribution, the other set had serrated boundaries and a trimodal γ' distribution. Progress has been made towards implementation of a suitable speckle pattern for digital image correlation (DIC). Quasi-isostatic room temperature tensile tests were performed in a scanning electron microscope, with images acquired at regular strain intervals. This preliminary data was qualitatively analyzed using Correlated Solutions VIC-2D software. The data for the serrated boundaries indicates that there are indeed interesting strain heterogeneities being developed that are related to grain orientations, boundary relationships to the tensile axis and other boundaries.

INTRODUCTION

With existing nickel-based superalloys it will be difficult to achieve the performance requirements of future turbine disc designs. This is due to conflicting property requirements at the bore (center) and rim of the disc. At the bore, strength and fatigue resistance are optimized with a fine-grained microstructure, while at the rim damage-tolerance and creep resistance are optimized with a coarse-grained microstructure [1]. For existing alloys and processing methods, these competing design requirements are extremely difficult to achieve using a single alloy composition and microstructure.

One method to address this problem is to develop hybrid superalloys that are both compositionally and microstructurally adaptable, that can tailored to meet the different temperature and stress demands required in different regions of the component [2, 3]. To exploit these new hybrid systems, physics-based computational methods are needed to predict material properties in the gradient regions, and describe material behavior during exposure to complex life cycles.

Currently, development of physics-based deformation models for high-temperature alloys systems is hindered by the type of validation data that can be provided via traditional testing techniques. Traditional tensile and creep tests determine averaged bulk properties, but provide limited insight into local deformation behavior. Even with post-testing microstructural evaluation, only a limited understanding can be gleaned relative to how local strain accommodation is controlled by variations in the microstructure. This makes it difficult to apply the experimental data collected to computational models of both traditional and hybrid alloys. Therefore, novel experimental techniques are required to characterize the local deformation fields produced during creep of these materials.

This paper highlights progress made towards the development and utilization of an in-situ, elevated-temperature tensile frame that operates inside of a scanning electron microscope to characterize the local deformation behavior in Ni-based superalloys. This work includes characterizing the microstructure of samples prior to testing, development of a speckle patterning technique for digital image correlation analysis of deformation fields, set-up of the test frame and preliminary results.

EXPERIMENTAL PROCEDURES

1.1 Materials

Prior to testing any hybrid alloys, in-situ testing procedures are being developed using a traditional Ni-based superalloy. The alloy selected was the γ' strengthened alloy Rene 104 (15wt% Cr,18.2% Co, 3.8%Mo, 1.9%W, 1.4%Nb, 3.5%Al, 3.5%Ti, 2.7%Ta, 0.03%C, 0.03%B, 0.05%Zr, bal Ni) [4]. Samples of Rene 104 were heat treated to produce samples with two different microstructures. The first heat treatment produced a "standard" microstructure consisting of relatively planar grain boundaries, while the second heat treatment produced a microstructure consisting of a serrated grain boundary structure, as shown in Figure 1 [5, 6]. Previous work has indicated that serrated boundaries have beneficial effects on fatigue crack growth resistance [6].

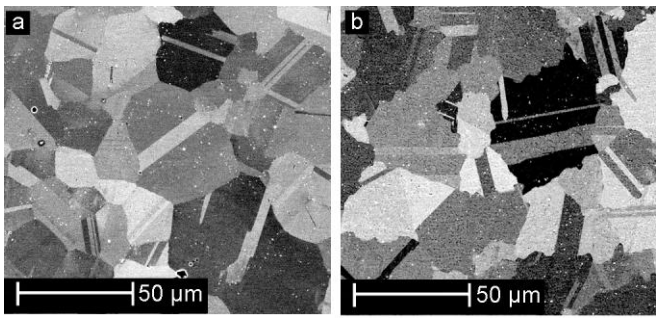

Figure 1. SEM backscatter electron images of the (a) standard heat treatment produces planar grain boundaries, (b) while the second heat treatment produces a serrated boundary structure.

1.2 Sample preparation

Following heat treatment, samples were electrical discharge machined to have a gage length of 1.78 cm, and nominal rectangular cross-section of 0.31 cm by 0.081 cm. Tensile samples were prepared for scanning electron microscopy (SEM) analysis using conventional polishing techniques, culminating with a final vibratory polish using 0.02 µm colloidal silica. Once polished, four microhardness indents were placed at the corners of a 0.01 cm^2 square centered in the middle of the gage section. These hardness indents indicate the location of the speckle pattern needed for in-situ testing, and assist in post-experiment registration of microstructural data with the local displacement maps. Other samples were prepared for γ' particle morphology and distribution analysis. These samples were cut parallel and perpendicular to the tensile loading direction and were mounted and polished similar to tensile samples. For these metallographic samples, after final polishing step the γ' particles were revealed using a selective etchant (2ml HF, 30ml HNO_3, and 50ml lactic acid).

1.2.1 Characterization techniques

Electron backscatter diffraction (EBSD) mapping was used to characterize grain size and grain orientation with respect to the tensile axis. EBSD was conducted on an FEI ESEM XL-30 SEM using EDAX TSL orientation image mapping system. Grains were defined as containing at least 5 data points, with less than 5° misorientation between adjacent data points. Twin boundaries of Σ3 orientation were not included in grain area calculations. Grain size distributions were determined using techniques developed by Payton for converting 2-dimensional grain information into 3-dimensional grain information [7]. Analysis of grain size distributions were conducted for each processing type using at least 2000 grains, ASTM standard E112 recommends at least 250 grains be counted to determine mean and standard deviation [8].

SEM images for particle analysis were conducted in an FEI Sirion XL-30 FEG-SEM nominally set at 15keV using ultra-high resolution, backscatter imaging mode. Particle size distributions were determined using image analysis techniques following procedures developed by Payton et al. [7, 9]. An average particle area was determined and linear particle size was calculated by converting area to cube length.

1.2.2 Speckle patterning

Correlated Solutions Inc. VIC-2D digital image correlation (DIC) software was used to analyze local deformation fields. In order to characterize intragranular deformation of the Rene 104 microstructure, digital images needed to be acquired at 1500x magnification, which necessitated the use of an SEM. Therefore, the speckle pattern needed for DIC had to be applicable for electron imaging. The DIC software produces optimum accuracy when the minimum speckle size is at least three pixels, and a greater number of speckles per grain produces a more detailed characterization of the strain distribution within each grain [10, 11]. Based on the typical pixel size of SEM images taken at the required magnification and limiting the image acquisition time to less than a minute in time, a random pattern was generated using square speckles with a size range between 0.25 and 0.6 μm.

Electron beam lithography was used to fabricate the desired pattern. This technique uses a focused scanning electron beam to locally expose photo-resist on the sample surface, which results in the point-by-point construction of the desired pattern [12]. Once exposed, the resist is developed and metal or dielectric can be deposited onto the sample surface. After deposition the developed resist is lifted off to reveal the pattern. Following standard clean-room procedures, 4 A PMMA resist was spin coated onto the sample surface. Once coated, the sample was exposed at 50 keV with a dose of 800 uC/cm^2 using a Vistec EBPG 5000 electron beam lithography machine. The resist was then developed in a 9:1 mixture of methyl isobutyl ketone and isopropyl alcohol. The location of the speckle pattern on the sample surface was determined by the microhardness indents placed on the surface before EBSD analysis, as shown in Figure 2. A Denton 502A evaporator was utilized to deposit 10nm of titanium followed by 140nm of gold onto the surface. Once coated the developed resist was lifted off the sample using an acetone bath, leaving a pattern of gold speckles on the sample surface, Figure 3.

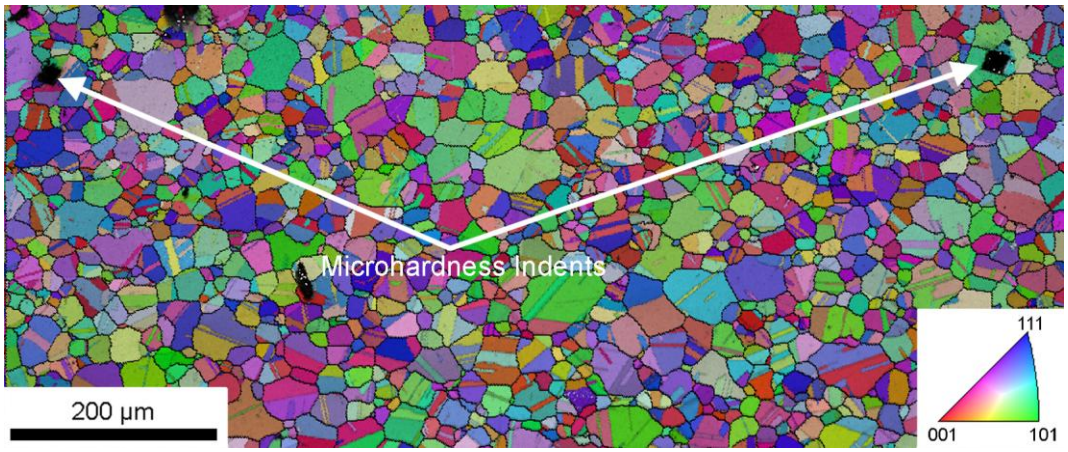

Figure 2. EBSD map of the standard heat treated microstructure showing the location of the microhardness indents used for applying the speckle pattern. In this image each color represents a particular crystal orientation as indicated by the inserted inverse pole figure.

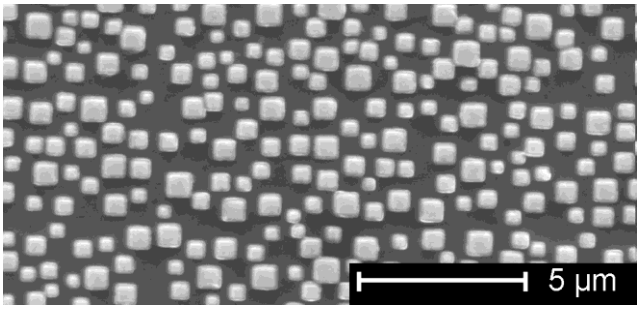

Figure 3. SEM secondary electron image of the Au speckle pattern created by e-beam lithography

1.3 Experimental test set-up

An Ernest Fullam® in-situ tensile stage was employed for this study. The stage is able to apply loads up to 4448 N, heat the specimen to temperatures up to 1200°C, provide measurements of load and crosshead displacement, and allows for EBSD acquisition while the sample is mounted in the test frame. The data acquisition system provided with the test frame was used to acquire load and displacement data every 30 seconds. Initial tensile testing was conducted at room temperature, and the total strain accumulated during each test was approximately 5% at a strain rate of $5x10^{-5}$ s^{-1}. Secondary electron images were collected at approximately 0.2% strain intervals. SEM operating parameters were as follows: 20kV accelerating voltage, dwell time of 10µsec, and an image size of 2048x1768 pixels, which corresponds to an image acquisition time of 37sec. Images were taken at 1000 and 1500x magnification at resolution of 6.7 or 10 pixels/µm.

Elevated temperature image acquisition capabilities of the SEM were tested by imaging a specimen which was incrementally heated to 600°C. At 100°C intervals the sample was held at temperature for 3 to 5 minutes before backscatter and secondary images were acquired using the same SEM operating parameters as discussed previously.

Correlated Solutions VIC-2D software was selected for conducting digital image correlation techniques for determining local strain distributions. Analysis was conducted using 35x35 pixel subset size and spacing between subset centers of 5 pixels. No distortion corrections were conducted for strain analysis, thus, the data presented in this paper is qualitative in nature.

RESULTS

1.4 Microstructural characterization

1.4.1 Grain size

The standard heat treatment produced an average 3-D grain size of 415 μm^2, while the serrated heat treatment produced and average 3-D grain size of 371 μm^2. The distribution of grain sizes is presented in Figure 4. The grain size distributions of these two processing types are very similar, indicating that the major difference between processing types are their boundary morphologies, as seen in Figure 1. The boundary serrations still need to be characterized in accordance with work by Mourer et al. [6].

1.4.2 γ' morphology and distribution

The standard heat treatment produced a bimodal γ' distribution consisting of spherical tertiary γ' precipitates that are typically less than 20 nm (true distribution undetermined), and cuboidal secondary γ' precipitates that are 160 ± 30 nm in width, Figure 5. The serrated heat treatment produced a trimodal γ' distribution with small spherical secondary γ' 86 ±18nm, large dendritic shaped γ' in the grain interiors, and globual γ' along the grain boundaries Figure 5.

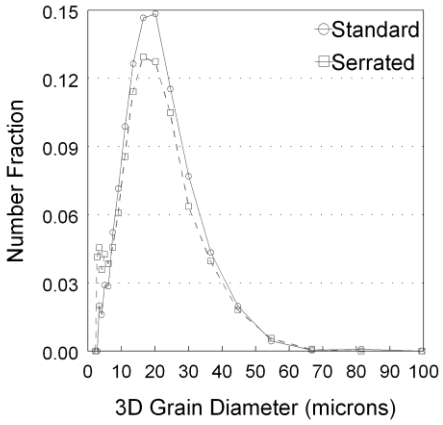

Figure 4. Grain size distributions for both the standard and serrated Rene 104 microstructures

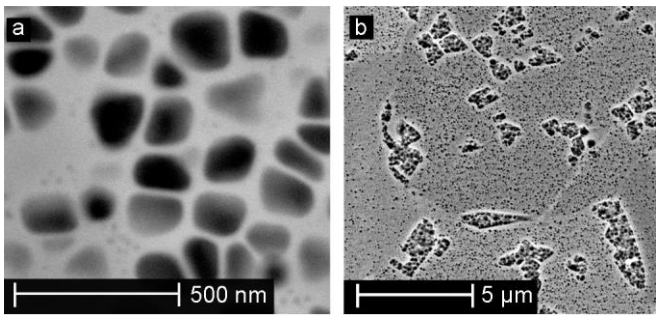

Figure 5. SEM backscatter images of the (a) bimodal γ' distribution of the standard microstructure as compared to the (b) trimodal γ' distribution of the serrated microstructure.

1.5 High temperature imaging

SEM imaging at incremental temperatures indicates that backscatter imaging in this microscope is only possible to about 300°C, above which thermal radiation causes excessive signal noise ratios – an effect which is consistent with other studies [13, 14]. Secondary images showed minimal visible degradation in quality up to 600°C, though specimen cleanliness is important consideration. Organic deposits on the sample surface (dirt, acetone, etc.) charge more readily at elevate temperature and obscure the true sample features. This experiment indicates that for elevated temperature testing above 300°C the speckle pattern for DIC must produce good secondary imaging contrast.

1.6 In-situ strain mapping

Bulk measurements of load and displacement were used to calculate the engineering stress and strain curve, which is shown in Figure 6. Here, sample displacement was obtained by measuring the cross-head displacement, and system compliance (i.e. elastic deflection of the load train) was not accounted for, thus, the stress-strain curves in Figure 6 are not accurate in the elastic regime. Nonetheless, the raw data shows that the serrated samples have higher yield strength then the standard samples by 10%.

Local strain data of the serrated sample, as calculated with the VIC-2D software, is presented for different bulk strain levels in Figure 7. The figure also shows the initial EBSD microstructure overlaid with the speckle pattern in the initial image, and the initial EBSD microstructural boundaries overlaid with the strain fields. None of the local strain levels at the end of the test are at or above the bulk strain levels calculated from crosshead displacement, indicating three possible problems: (a) the load cell is compliant and contributing to the cross-head displacement readings, (b) the sample slipped in the grips during testing, and or (b) spatial and drift distortions in the SEM images are high enough to cause inaccuracy in the quantitative assessment of local strain measurements [15, 16].

Qualitatively, the local strain field maps indicates that some of the grain triple points act as strain localization sites, while other triple points show no appreciable strain build-up. The calculated Schmid factors for the grains oriented for {111}<110> slip under tensile loading along the horizontal axis indicates that due to the high symmetry of the face centered cubic system very few grains are oriented for hard slip, with low Schmid factors. This is indicated by grains that are blue or green in color in Figure 8 (b). With this limited data set, it is seen that most regions of no deformation occur at triple points, or boundaries between favorably and unfavorably oriented grains. There does not appear to be as definitive relationship between areas of maximum strain, but grain boundaries appear to play a dominant role. A more detailed analysis of grain orientations is needed to determine correlations between strain field characteristics and local microstructure.

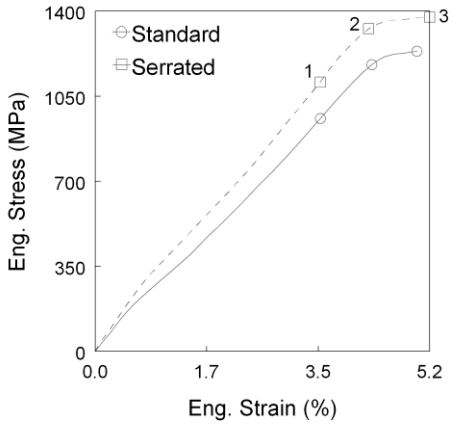

Figure 6. Bulk stress-strain data for standard and serrated heat treated samples

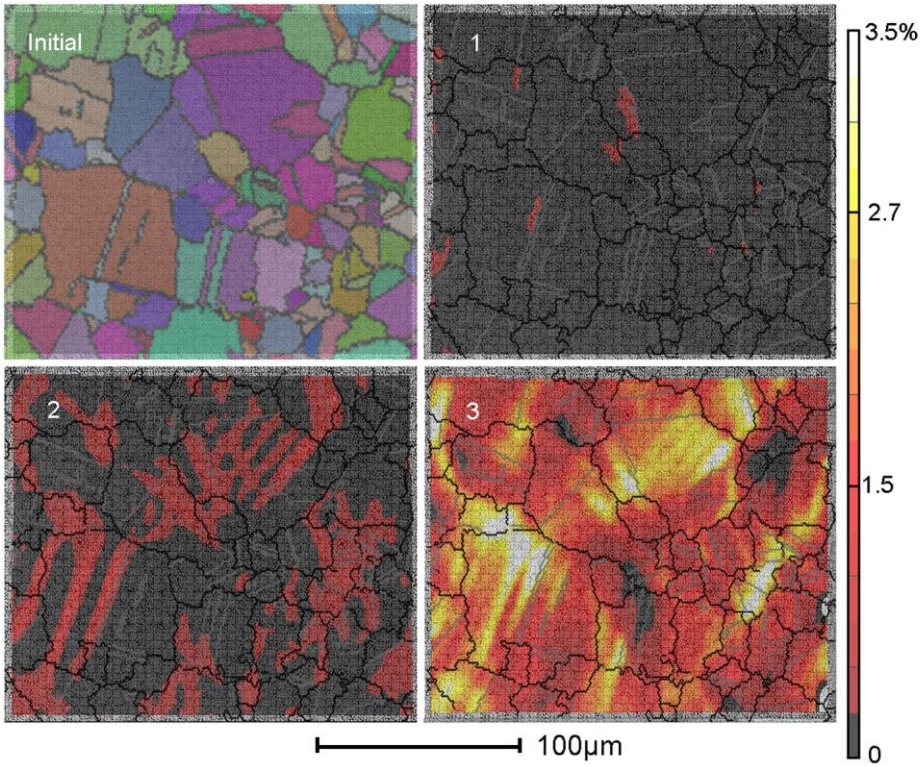

Figure 7. Local strain maps overlaid with the initial EBSD grain information (e_{xx}) at selected points along the stress-strain curve shown in Figure 6. bulk strain levels (as indicated in Figure 6). The loading direction is along the x-axis

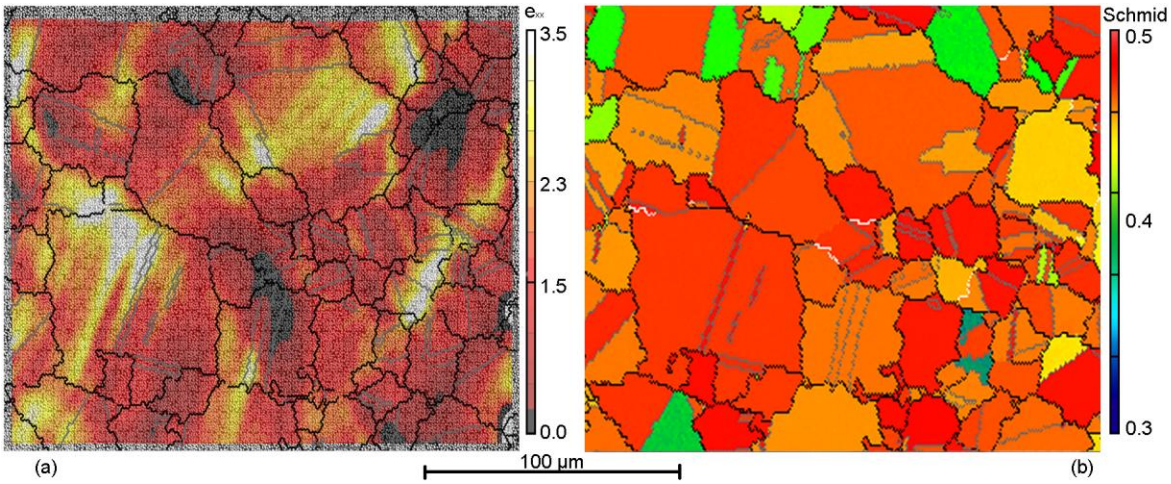

Figure 8 (a) Final strain distribution as compared with the (b) Schmid factor for {111}<110> slip. Blue and green grains are those that have low Schmid factors for octahedral slip

CONCLUSIONS

The ambient temperature data shows there are strain heterogeneities observed in this alloy at the grain size level that cannot be directly linked to Schmid factors. There appears to be a relationship between the extreme strain values and proximity to grain boundaries and grain boundary triple points, this is consistent with another ambient temperature study on a similar nickel based superalloy [17]. Future work includes set-up of the resistance heating equipment for conducting high temperature experiments, 600-800°C. For these high temperature conditions slip by {111} <112> partial dislocations should be predominate.

This study also indicates that the lithography pattern created was too dense to facilitate imaging at low enough magnifications to have a statistically significant representation of grain orientations and grain boundary triple points. At lower magnifications the discreet pattern was not longer recognizable and interference fringes are produced. The lithography pattern needs to be optimized to allow for SEM images at desired magnifications and testing temperatures. In addition, we would like to develop procedures for depositing hafnia speckle patterns, in order to have a pattern that is compatible with high-temperature testing between 600 and 800°C, as other studies have shown that gold and platinum speckles exhibit transient behavior on the surface of Ni-based superalloys at temperatures above 500°C [18]. Another needed modification is the placement of special markers (numbers, different shapes, etc) to help the researcher manually overlay the strain images with EBSD grain images taken after testing. Also, a series of lines parallel and/or perpendicular to the tensile axis needs to be added if grain boundary sliding contributions are to be examined [19].

Following calibration of the equipment for high temperature testing using conventional nickel based superalloys, the system will be utilized to probe heterogeneities in hybrid nickel based superalloys. Testing will be conducted on two different hybrid alloys, a dual heat treatment turbine disc and a bonded turbine disc [3, 4]. The dual heat treatment disc has a very shallow microstructural gradient, while the bonded disc has a very sharp microstructural gradient. This full field in-situ technique should help facilitate better understanding and in turn modeling of deformation behavior in these gradients in microstructures.

ACKNOWLEDGEMENTS

This work is funded by the Air Force Research Laboratory (AFRL) STW-21 program. The author would like to thank Aimee Bross of the Ohio State University Nanotechnology Center for her invaluable assistance with development on the lithography techniques for the speckle patterning. The support received from the Materials & Manufacturing Directorate of the Air Force Research Laboratory has been instrumental for the development of the in-situ tensile frame.

REFERENCES

1. J. Gayda, et al., *The Effect of Dual Microstructure Heat Treatment on an Advanced Nickel-Base Disk Alloy*, in Superalloys, pp.323-329, (2004).
2. D. P. Mourer, et al., *Dual Alloy Disk Development*, in Superalloys, pp.637-643, (1996).
3. D. P. Mourer and J. L. Williams, *Dual Heat Treat Process Development for Advanced Disk Applications* in Superalloys, pp.401-407, (2004).
4. R. C. Reed, *The Superalloys: Fundamentals and Applications*, Cambridge University Press, (2006).
5. H. L. Danflou, et al., *Mechanisms of Formation of Serrated Grain Boundaries in Nickel Base Superalloys*, in Superalloys 1996, pp.119-127, (1996).
6. H. L. Danflou, et al., *Formation of Serrated Grain Boundaries and Their Effect on the Mechanical Properties in a P/M Base Superalloy*, in Superalloys 1992, pp.63-72, (1992).
7. E. J. Payton, *Characterization and Modeling of Grain Coarsening in Powder Metallurgical Nickel-Based Superalloys*, PhD Thesis, The Ohio State University, (2009)
8. ASTM committee E04.08, *ASTM E112-Standard Test Methods for Determining Average Grain Size*, in ASTM Standards, pp.1-26, (1996).
9. E. J. Payton, et al., *Semi-automated Characterization of the gamma prime phase in Ni-based superalloys via high-resolution backscatter imaging*, in Mat. Sci. and Eng. A, **Vol. 527** pp. 2684-92, (2009)
10. W. A. Scrivens, et al., *Development of Patterns for Digital Image Correlation Measurements at Reduced Length Scales*, in Experimental Mechanics, **Vol. 47** (1), pp. 63-77, (2007)
11. M. A. Sutton, et al., *Image Correlation for Shape, Motion and Deformation Measurements*, Springer, (2009).
12. C. Zheng, *Nanofabrication: Principles, Capabilities and Limits*, Springer Inc., (2008).
13. I. M. Fielden, *Investigation of Microsctural Evolution by Real-Time SEM of High-Temperature Specimens*, Sheffield Hallam University (2005)
14. G. G. E. Seward, et al., *High-temperature electron backscatter diffraction and scanning electron microscopy imaging techniques: In-situ investigations of dynamic processes*, in Scanning, **Vol. 24** pp. 232-240, (2002)
15. M. A. Sutton, et al., *Scanning Electron Microscopy for Quantitative Small and Large Deformation Measurements - Part II: Experimental Validation for Magnifications from 200 to 10,000*, in Experimental Mechanics, **Vol. 47** (6), pp. 789-804, (2007)
16. M. A. Sutton, et al., *Scanning Electron Microscopy for Quantitative Small and Large Deformation Measurements - Part I: SEM Imaging at Magnifications from 200 to 10,000*, in Experimental Mechanics, **Vol. 47** (6), pp. 775-787, (2007)
17. M. A. Tschopp, et al., *Microstructure-Dependent Local Stain Behavior in Polycrystals Through In-Situ Scanning Electron Microscope Tensile Experiments*, in Met. Mat. Trans. A, **Vol. 40A** pp. 2363-68, (2009)
18. A. Soula, et al., *Grain boundary and intragranular deformations during high temperature creep of PM Ni-based superalloys*, in Superalloys 2008, pp.387-93, (2008).
19. R. C. Gifkins, *The Measurement of Grain-Boundary Sliding in Polycrystalline Specimens*, in Metal Sci. J., **Vol. 7** pp. 15-19, (1973)